Sheffield Hallam University

Effect of long-term gaseous hydrogen exposure on the static and fatigue behaviour of T700/VTC401 unidirectional laminates

WANG, H <http://orcid.org/0009-0008-8043-105X>, ABBASIAN, T <http://orcid.org/0009-0001-1620-1443>, JANANI, R <http://orcid.org/0000-0002-3633-0488>, SKOF, M <http://orcid.org/0000-0002-7130-164X>, ROBERT, C, Ó BRÁDAIGH, CM <http://orcid.org/0000-0002-8048-4222>, SCENINI, F <http://orcid.org/0000-0002-8974-4860> and SUSMEL, L <http://orcid.org/0000-0001-7753-9176>

Available from Sheffield Hallam University Research Archive (SHURA) at:

https://shura.shu.ac.uk/37785/

This document is the Accepted Version [AM]

Citation:

WANG, H, ABBASIAN, T, JANANI, R, SKOF, M, ROBERT, C, Ó BRÁDAIGH, CM, SCENINI, F and SUSMEL, L (2026). Effect of long-term gaseous hydrogen exposure on the static and fatigue behaviour of T700/VTC401 unidirectional laminates. International Journal of Hydrogen Energy, 261: 156781. [Article]

Copyright and re-use policy

See http://shura.shu.ac.uk/information.html

Sheffield Hallam University Research Archive
http://shura.shu.ac.uk

Effect of long-term gaseous hydrogen exposure on the static and fatigue behaviour of T700/VTC401 unidirectional laminates

H. Wang[1], T. Abbasian[2], R. Janani[3], M. Skof[3], C. Robert[2], C. Ó Brádaigh[2], F. Scenini[4,5], and L. Susmel[3]

[1]School of Mechanical, Aerospace and Civil Engineering, The University of Sheffield, Mappin Street, Sheffield S1 3JD, UK
[2]School of Chemical, Materials and Biological Engineering, The University of Sheffield, Mappin Street, Sheffield S1 3JD, UK
[3]School of Engineering and Built Environment
Sheffield Hallam University, Harmer Building, Sheffield, S1 1WB, UK
[4]Metallurgy and Corrosion, Department of Materials, The University of Manchester, Manchester M13 9PL, UK
[5]Royce Institute, The University of Manchester, Manchester, M13 9PL, UK

Corresponding author: Professor **Luca Susmel**
School of Engineering and Built Environment, Sheffield Hallam University,
Harmer Building, Sheffield, S1 1WB, United Kingdom
email: l.susmel@shu.ac.uk

Abstract

The long-term effects of gaseous hydrogen exposure on the mechanical performance of carbon-fibre-reinforced polymers (CFRPs) remain poorly understood. This study investigates the static and fatigue behaviour of T700/VTC401 $[0]_2S$ carbon-fibre-reinforced epoxy laminates after exposure to hydrogen at 6 bar and room temperature for 10 months. Static tensile tests showed no statistically significant changes in elastic modulus or ultimate tensile strength. In contrast, tension–tension fatigue tests (R = 0.1, 10 Hz) revealed a reduction in fatigue resistance, with an approximately 10% decrease in the fatigue strength corresponding to $2{\cdot}10^6$ cycles and a flatter S-N response. Optical microscopy, Raman spectroscopy, and secondary electron microscopy did not identify hydrogen-specific damage features, suggesting that the observed fatigue degradation resulted from subtle changes in matrix and fibre–matrix interfacial behaviour. The results demonstrate that prolonged exposure to low-pressure gaseous hydrogen can reduce fatigue performance while leaving static tensile properties largely unaffected.

Keywords: carbon/epoxy laminate; hydrogen; fatigue; static strength

NOMENCLATURE

k	negative inverse slope
E	elastic modulus
N_f	number of cycles to failure
N_A	reference number of cycles to failure
R	load ratio (R=$\sigma_{min}/\sigma_{max}$)
T_σ	scatter ratio
σ_{UTS}	ultimate tensile strength
$\sigma_{A,90\%}$	endurance limit amplitude for a probability of survival of 90%
$\sigma_{A,50\%}$	endurance limit amplitude for a probability of survival of 50%
$\sigma_{A,10\%}$	endurance limit amplitude for a probability of survival of 10%
σ_{min}	minimum stress in the cycle
σ_{max}	maximum stress in the cycle
$\Delta\sigma$	stress range ($\Delta\sigma = \sigma_{max} - \sigma_{min}$)

1. Introduction

Hydrogen technologies are central to the decarbonisation of transport, energy storage, and industrial processes, driving the deployment of lightweight, high-performance structural materials capable of operating under demanding mechanical and environmental conditions. In this context, carbon-fibre-reinforced polymers and glass-fibre-reinforced polymers play a pivotal role thanks to their high specific strength and stiffness, excellent corrosion resistance, and design flexibility. These attributes make fibre-reinforced composites attractive not only for high-pressure containment systems, but also for a broader range of hydrogen-related applications, including pipelines, pressure vessels, load-bearing structures, and components exposed to cyclic pressurisation and variable temperatures. As hydrogen infrastructures scale up, understanding the mechanical integrity and long-term durability of these composite systems becomes a key enabling requirement [1].

Most of the existing knowledge on the interaction between hydrogen and composite materials has been generated in the context of hydrogen storage tanks [2-12]. These studies have provided invaluable insight into structural performance, qualification protocols, and safety margins under realistic service conditions. The focus on tanks has also shaped the way damage mechanisms are interpreted, however, often embedding assumptions that are specific to vessel architectures, liners, and operating scenarios. As a result, the transferability of this knowledge to composite structures more generally - where stress states, exposure histories, and damage evolution may differ - remains limited [1, 13].

From a materials perspective, fibre-reinforced composites operating in hydrogen environments are susceptible to a range of interacting fatigue and failure mechanisms [9, 10, 14, 15]. Under cyclic loading, damage may involve fibre breakage, matrix cracking, fibre–matrix interfacial debonding, and their combined evolution. Hydrogen exposure can accelerate these processes by diffusing through the composite, particularly along micro-cracks, interfaces, and manufacturing-induced defects such as porosity, voids, and local delaminations [10, 15-17]. These microstructural imperfections act as preferential sites for damage initiation and growth, leading to a progressive reduction in both static and fatigue strength [18]. Operational factors - most notably pressure cycling, temperature fluctuations, and rapid pressurisation - further complicate the response, promoting damage accumulation and altering the relative contribution of different mechanisms [2, 4, 6]. While these effects have been extensively documented in hydrogen storage systems [6, 19], they reflect more general material behaviours that are also relevant to composite components beyond tank applications.

Although several studies have examined the performance of composites in hydrogen storage vessels [2, 4-6], comparatively little is known about how long-term hydrogen pre-exposure affects subsequent static and fatigue behaviour, particularly in unidirectional laminates. In addition, the governing damage mechanisms may differ between (i) hydrogen pre-soaking followed by mechanical loading and (ii) the simultaneous action of hydrogen ingress and cyclic stresses, where coupled physical and chemical effects can lead to different degradation pathways. Given the non-linear, saturating nature of hydrogen absorption in epoxy matrices, even relatively low pressures such as 6 bar can result in meaningful hydrogen uptake, making pre-exposure tests valuable for isolating intrinsic material responses.

Against this background, the present study aims to quantify the effect of long-term, low-pressure hydrogen pre-soaking on the static and fatigue behaviour of a T700/VTC401 $[0]_{2s}$ unidirectional laminate and to assess whether such exposure produces measurable mechanical degradation or identifiable changes in surface or fracture morphology.

2. Material, fabrication of the specimens and hydrogen soaking

2.1. Material

The composite laminates used in the present investigation were fabricated from unidirectional (UD) T700-12K carbon fibre prepreg containing VTC401 epoxy resin system supplied by SHD Composite Materials Ltd. The prepreg had a nominal fibre weight of 124 g/m^2 and a resin content of 38% by weight. For specimen testing, FR-4 glass-epoxy end tabs (1.56 mm thick, Vector Electronics & Technology, Inc.) were bonded to the laminates using XA120 film adhesive supplied by Easycomposites Ltd.

2.2. Laminate Fabrication and Cure figure

A toughened glass plate was used as the mould surface. The mould was first cleaned with acetone and then a release agent (CR1 Easy-Lease, EasyComposites Ltd.) was applied according to the manufacturer's instructions. Four plies of the carbon fibre prepreg were cut into 300 mm × 300 mm panels. The plies were stacked sequentially to create a balanced $[0]_{2s}$ laminate, with all fibres aligned in the 0° direction.

The lay-up was prepared for curing using a standard vacuum bagging sequence of prepreg (Fig. 1A), release film (VAClease20R1.2, VAC Innovation Ltd – Fig. 1B), polyester breather fabric (BR180, EasyComposites Ltd.), and vacuum bag film (VB200, EasyComposites Ltd – Fig. 1C). The assembly was sealed with vacuum sealant tape (ST150, EasyComposites Ltd.). A vacuum of at least -0.9 bar was applied, and a vacuum drop test was performed for 15 minutes to ensure bag integrity. Curing was performed in an autoclave (Fig. 1D) under 6 bar of external applied pressure. The thermal cure cycle was as follows:

- Ramp from 25°C to 80 °C at 2°C/min.
- Hold at 80°C for 10 minutes.
- Ramp from 80°C to 120°C at 2 °C/min.
- Hold at 120°C for 45 minutes.
- Cool to room temperature at a controlled rate of ≤3°C/min to below 40 °C.

2.3. Specimen Preparation

The final measured thickness of the cured laminates was between 0.55 mm and 0.62 mm. Bonding surfaces were lightly abraded by hand prior to cleaning with isopropanol and application of the adhesive film. The end-tabs were bonded using a vacuum bag oven process. The oven cycle consisted of a 2 °C/min ramp to 90 °C, followed by an 8-hour hold. The tabbed panels were machined into coupons with approximate dimensions of 100mm × 10mm with a 30mm gauge length following the cutting plan shown in Fig. 2. An initial cut was made using a water jet leaving the specimens joined by the edges of the tab area. The final cuts were completed with a diamond saw under water cooling. Finally, the specimen edges were polished to a 1200 grit finish to remove any machining marks.

2.4. Hydrogen soaking procedure

The T700/VTC401 $[0]_{2s}$ specimen set was divided into two groups, with half of the coupons subjected to long-term gaseous hydrogen exposure prior to mechanical testing and the remainder retained in laboratory air as unsoaked references. Hydrogen charging was performed in a dedicated stainless-steel pressure tube (Fig. 3) using high-purity hydrogen (≥ 99.999%). Prior to pressurisation, the chamber was purged several times with hydrogen to minimise the presence of oxygen and moisture. It was then brought to a nominal pressure of 6 bar and maintained under laboratory ambient conditions for an exposure period of 10 months, during which the temperature remained within the range 20–25 °C. Pressure measurements taken during storage indicated that the hydrogen pressure remained close to the nominal value, with fluctuations not exceeding approximately ±0.3 bar. These

conditions were chosen to represent long-term service in a low-pressure gaseous hydrogen environment.

After exposure, the specimens were recovered, visually checked to exclude obvious damage and transferred to liquid-nitrogen storage to minimise hydrogen desorption prior to testing. The mechanical tests were then performed sequentially, such that the storage duration in liquid nitrogen varied between specimens. In the most extreme case, the final specimen tested remained in liquid-nitrogen storage for approximately three weeks.

Before mechanical testing, each specimen was removed from the liquid nitrogen and allowed to warm naturally under laboratory ambient conditions. The total time elapsed between extraction from liquid nitrogen and the start of the mechanical test was approximately 15 minutes. Surface temperature measurements performed using an infrared thermometer confirmed that this period was sufficient for the specimens to return to room temperature prior to testing. All static and fatigue tests on hydrogen-soaked specimens were carried out using identical mechanical test protocols for unsoaked and hydrogen-soaked coupons so that hydrogen effects could be assessed by direct comparison.

Given that cryogenic storage may itself induce thermal stresses within the polymer matrix, a small set of LN_2-only control specimens (i.e., specimens not exposed to hydrogen) was also stored in liquid nitrogen and subsequently tested following the same handling and warming procedure adopted for the hydrogen-soaked coupons. The objective was to assess whether the storage protocol could introduce any measurable changes in mechanical performance. To this end, one static tensile test and three fatigue tests were performed. The static test yielded a tensile strength well within the scatter band of the results reported in Table 1 for the un-soaked material. Similarly, the fatigue verification tests comprised two specimens tested in the medium-cycle fatigue regime, both failing after approximately 10^4 cycles to failure, and one specimen tested in the high-cycle fatigue regime, failing after approximately 10^6 cycles to failure. All three fatigue results were found to fall within the scatter band defined by the fatigue data obtained for the un-soaked reference material.

Overall, these control verification tests showed no evidence that storage in liquid nitrogen, followed by warming to room temperature prior to testing, introduced measurable damage or influenced the static or fatigue behaviour of the investigated CFRP laminate.

3. Static behaviour under tensile loading

Static tensile tests were performed on three unsoaked and two hydrogen-soaked specimens using a 250 kN servo-hydraulic static and dynamic universal testing machine, in accordance with ASTM D3039/D3039M for unidirectional fibre-reinforced polymer matrix composites [20]. The static tensile specimens had a nominal width of 10mm and a nominal thickness of 0.6mm. Specimens were aligned with the loading axis parallel to the fibre direction (0°), and hydraulic wedge grips were employed to ensure stable load application and to minimise grip-induced damage. All tests were conducted at room temperature in air under displacement control with a crosshead speed of 1 mm/min. Axial displacement in the gauge region was measured using a clip-on extensometer with a 12.5 mm gauge length attached at the specimen centre. Each specimen was monotonically loaded in tension under displacement control until failure, and the elastic modulus and ultimate tensile strength were determined by post-processing the recorded force-displacement data.

Stress–strain curves were generated for both unsoaked and hydrogen-soaked specimens. Two representative stress–strain curves for an unsoaked laminate specimen (Test No. 1) and an H_2-soaked laminate specimen (Test No. 4) are reported in Fig. 4a and Fig. 4b, respectively. These curves show two representative examples of the collected data, with the static mechanical properties of all tested specimens summarised in Table 1. For the unsoaked laminates, the fibre-direction elastic modulus ranged from 105.2 to 120.8 GPa,

with ultimate tensile strengths in the range 1818.7–2193.6 MPa. For the hydrogen-soaked specimens, the elastic modulus ranged from 106.0 to 115.4 GPa, and the ultimate tensile strengths from 2187.6 to 2222.8 MPa. Owing to the limited number of specimens, no further statistical analysis was performed or reported; the objective of this preliminary investigation was to detect any evident change in static behaviour induced by hydrogen soaking, rather than to quantify static material properties rigorously using a statistically significant dataset under unsoaked and hydrogen-soaked conditions.

Overall, these results indicate that long-term hydrogen soaking under the investigated conditions did not produce any significant change in the static tensile behaviour of the T700/VTC401 $[0]_{2s}$ laminate at the coupon scale. Within the bounds of experimental scatter, the laminates exhibited essentially unchanged stiffness, strength, and ductility, with only marginal differences observed between unsoaked and hydrogen-soaked specimens. Although the number of tests was limited, the repeatability of the measurements was considered satisfactory, as the scatter exhibited by the hydrogen-soaked specimens was comparable to that observed for the unsoaked material and all measured properties remained within the same overall range. Consequently, no systematic trend indicative of hydrogen-induced degradation of the static tensile response could be identified.

4. Fatigue behaviour

Fatigue tests were performed at room temperature in air using a 250 kN servo-hydraulic static and dynamic universal testing machine, following the general procedures of the tension–tension fatigue methodology of ASTM D3479/D3479M for polymer matrix composite materials [21]. Constant-amplitude tension–tension sinusoidal loading was applied under load control with a stress ratio, $R = \sigma_{\min}/\sigma_{\max}$, equal to 0.1 and a cyclic loading frequency of 10 Hz [22]. To monitor possible temperature variations at this frequency, a calibration specimen was tested to complete fracture at a stress range of 1800 MPa (i.e., the highest stress range considered), with the surface temperature recorded at one-minute intervals for 23 minutes using an infrared thermometer. As no evident temperature variation was observed and the temperature remained consistently at room temperature, no active cooling was employed during testing. For each selected stress level, specimens in both the unsoaked and hydrogen-soaked conditions were tested to failure. The number of cycles to failure, N_f, was recorded for each specimen and subsequently used to construct the corresponding S–N curves. Failure was defined as complete separation of the fatigue specimens.

The experimental S-N results were post-processed by assuming a log-normal distribution of the number of cycles to failure at each stress level, with the confidence level set to 95% [23-25]. Using this standard approach, three parameters were calculated to quantify the fatigue strength under unsoaked and hydrogen-soaked conditions: (i) the inverse negative slope, k; (ii) the endurance limit range, $\Delta\sigma_{A,50\%}$, corresponding to a probability of survival (P_S) of 50%, evaluated at a reference number of cycles to failure $N_A = 2 \times 10^6$; and (iii) the scatter ratio, T_σ, defined as the ratio between the endurance limits at $N_A = 2 \times 10^6$cycles to failure for 10% and 90% probabilities of survival. These parameters were employed to model the S–N behaviour using the following standard equation:

$$\Delta\sigma^k \cdot N_f = \Delta\sigma_A^k \cdot N_A \quad (1)$$

Within the adopted statistical framework, the endurance limit is defined as the fatigue strength corresponding to $N_A = 2 \times 10^6$cycles to failure, as determined from the fitted S-N relationship.

Fig. 5 shows the S-N curves (plotted in terms of stress range, $\Delta\sigma = \sigma_{max} - \sigma_{min}$) for unsoaked and hydrogen-soaked laminates, together with the corresponding scatter bands

determined for survival probabilities of 10% and 90%. For the unsoaked condition, the statistical analysis yielded (see also Fig. 5) an inverse slope, k, equal to 45, an endurance limit, $\Delta\sigma_{A,50\%}$, of 1570.8 MPa, and a scatter ratio, T_σ, equal to 1.161. For the hydrogen-soaked condition, the corresponding values were $k = 59.6$, $\Delta\sigma_{A,50\%} = 1418.4$ MPa, and $T_\sigma = 1.135$. Overall, hydrogen soaking resulted in an approximately 10% reduction in the endurance limit.

Turning to the slope of the fatigue curves, the increase in the inverse slope parameter k from 45 for the unsoaked condition to 59.6 for the hydrogen-soaked condition indicates a flatter S–N response in the medium-cycle fatigue regime. From a practical standpoint, this implies that the detrimental effect of hydrogen becomes increasingly pronounced as the operating conditions shift towards the medium- to low-cycle fatigue regime.

With regard to statistical dispersion, the scatter ratio changes only marginally, decreasing from $T_\sigma = 1.161$ in the unsoaked condition to $T_\sigma = 1.135$ after hydrogen soaking. The negligible variation observed between the two conditions suggests that, while hydrogen exposure had a detrimental effect on the overall fatigue strength, it did not introduce a significant increase in fatigue life scatter for the laminate and loading configuration considered.

It is also worth noting that the approximately 10% reduction in endurance limit may appear relatively modest when considered in isolation. However, the observed shift is consistent across the entire S-N response and is accompanied by a measurable increase in the inverse slope parameter, indicating a systematic reduction in fatigue resistance rather than an isolated change at the endurance limit. Owing to the relatively limited number of fatigue tests available [25], no formal statistical hypothesis testing was performed to assess the statistical significance of the difference between the two fatigue curves. Consequently, the present results should be interpreted as evidence of a clear and repeatable trend towards reduced fatigue performance following hydrogen exposure, rather than as a precise quantification of the magnitude of the effect. Further testing using a larger dataset would be required to establish the statistical significance of the observed reduction with a high degree of confidence.

With regard to repeatability, it should be noted that the fatigue characterisation was performed using multiple specimens tested at several stress levels and the resulting S-N curves were analysed according to ASTM E739 [23]. As is well known, fatigue data inherently exhibit a degree of scatter, which is explicitly accounted for by the statistical procedures prescribed by the standard. In the present investigation, the scatter ratios obtained for the unsoaked and hydrogen-soaked conditions were very similar ($T_\sigma = 1.161$ and $T_\sigma = 1.135$, respectively), indicating a comparable level of variability in the two datasets. This observation suggests that the fatigue results were reasonably repeatable and that hydrogen exposure did not introduce any appreciable increase in data scatter. Rather, the principal effect of hydrogen soaking was a systematic reduction in fatigue strength, reflected by both the lower endurance limit and the flatter S-N response.

5. Macro-/Microscopic observations of surface and fracture morphology

Microscopic examinations were performed on the outer surfaces and fracture surfaces of unsoaked and hydrogen-soaked T700/VTC401 $[0]_{2s}$ laminates in order to identify any possible hydrogen-induced changes or alterations.

Initially, observations were carried out using a Nikon optical microscope at magnifications of 5×, 10× and 20×. Representative images of the tool-face and bag-face surfaces after testing are shown in Fig. 6 and Fig. 7, respectively, while Fig. 8 presents representative fracture surfaces under fatigue loading for unsoaked and hydrogen-soaked specimens.

For the as-tested laminate surfaces, both unsoaked and hydrogen-soaked specimens exhibited comparable microstructural features across all examined magnifications and observation areas. In particular, no systematic differences were observed in fibre alignment, surface resin coverage, or the distribution of manufacturing-related features. Furthermore, optical microscopy did not reveal any evidence of hydrogen-specific damage, such as surface blistering, extensive micro-cracking, or local debonding, within the resolution limits of the technique. It should be noted that the present observations are qualitative in nature; therefore, subtle differences that might be revealed through dedicated quantitative surface characterisation techniques cannot be excluded.

The fracture surfaces likewise showed no qualitative differences between unsoaked and hydrogen-soaked specimens, for either static or fatigue tests. In both conditions, the failure morphology was dominated by fibre breakage, together with regions of fibre–matrix debonding, matrix cracking and limited fibre pull-out, consistent with the well-established tensile failure morphology of unidirectional carbon/epoxy laminates reported in the literature [26]. The overall fracture topography, including the relative proportions of flat fibre fracture, hackle-like matrix features and exposed fibre bundles, was similar for soaked and unsoaked coupons.

Since, within the resolution of the above observations, hydrogen exposure did not give rise to distinctive microstructural or fractographic signatures at the laminate surface or on the final fracture plane, further analyses were performed using Raman spectroscopy and secondary electron microscopy, as discussed in what follows.

Soaked and unsoaked fatigue specimens (VTC-11-1750, VTCH3-1500) were analysed using an inVia Raman spectrometer with an automated stage (Renishaw, UK) and a 785 nm diode laser. Line maps were acquired in duplicate along the length of the carbon fibre composites at 50 μm intervals (10 spots), using a x20 objective (spot size ~2.4 μm) at 5% laser power (~198 mW at 100%). Two accumulations were collected and co-added per spot. All spectra were linearly baseline-corrected and smoothed using WiRE software (v3.4). Fig. 9 presents representative areas selected for Raman mapping.

Representative individual Raman spectra along the line maps for both unsoaked and hydrogen-soaked composites are shown in Fig. 10. The spectral features were consistent both across each map and between different regions within each sample.

Raman spectra, presented as the mean spectrum for each line map, are shown in Fig. 11. The mean spectrum represents the average of all spectra collected across each mapped region, providing a representative profile of the chemical structure for that sample. The two broad and strong bands between 1340 and 1600 cm^{-1} correspond to the D and G bands of the embedded carbon fibres. Characteristic bands of the epoxy aromatic backbone appear at 640, 820, and 1140 cm^{-1}, corresponding to out-of-plane deformation, bending, and in-plane C-H vibrations, and at 1188 and 1610 cm^{-1}, associated with vibrations of C-O, C=C, and C-C groups within the epoxy resin [27, 28]. These features were consistent between the two samples with no discernible shifts or changes in the band ratios indicating no noticeable chemical changes induced by long-term exposure to hydrogen. This observation is in line with the expected interaction mechanism between hydrogen and the composite. Any defect associated with hydrogen exposure is likely linked to decompression of the diffused hydrogen causing local interfacial debonding, or microcracking which do not lead to chemical changes detectable by Raman. As a result, the Raman data support the chemical stability of both carbon fibre and epoxy resin under the high exposure conditions.

Subsequently, the investigation was further extended using secondary electron microscopy. Images of fracture surfaces were acquired via an FEI Quanta 650 scanning electron microscope with Everhart Thornley detector (ETD), using an acceleration voltage of 5 kV. Before analysis, a segment was cut from the specimens. The cut sample was vertically

mounted using stainless-steel springs and subsequently sputter coated with carbon to prevent charge build-up during analysis. SEM micrographs are shown in Figs 12a and 12b. All samples exhibit fibre-matrix debonding, irrespective of hydrogen exposure and type of loading. The SEM micrographs furthermore show holes in the polymer due to fibres having been pulled out of the matrix during the test. This effect was also observable in all samples. The sharp fracture surfaces of the matrix material are typical of brittle fracture behaviour [9]. Hydrogen exposure does not seem to worsen fibre pull-out, fibre/matrix debonding or matrix cracking on a qualitative scale in the analysed specimens.

All characterisation analyses discussed in the present section indicate that the reduction in fatigue endurance identified was not accompanied by obvious changes in macroscopic or microscopic material morphology and fracture surface appearance.

Overall, the absence of hydrogen-specific features in the optical, Raman, and SEM analyses indicates that hydrogen does not produce macroscopic or microscopically identifiable damage in either the fibres or the matrix. Instead, its influence is likely confined to subtle changes in the matrix and the fibre–matrix interface that accelerate the early stages of fatigue damage. While the present fractographic observations were intended to provide qualitative evidence of the dominant failure mechanisms, future studies incorporating a quantitative assessment of fibre pull-out lengths and interfacial debonding areas may help establish more direct correlations between microscale damage processes and the observed reduction in fatigue endurance.

A possible explanation is that hydrogen exposure promotes the formation or exacerbation of localised defects within the polymer matrix and at the fibre–matrix interface, which represent the regions most susceptible to hydrogen uptake and transport within CFRP systems. In particular, phenomena such as polymer matrix plasticisation and cavitation induced by hydrogen desorption during decompression may contribute to the development of internal damage features, including microvoids and interfacial degradation [29, 30]. To investigate the possible occurrence of such effects, optical microscopy, Raman spectroscopy, and secondary electron microscopy were employed. These techniques were selected because they are capable of identifying hydrogen-induced changes over a range of length scales, including matrix cracking, void formation, fibre–matrix debonding, fracture-surface features, and possible alterations in the chemical structure of the polymer matrix. Although no significant differences were detected between the soaked and unsoaked conditions, this finding remains important, as it indicates that hydrogen exposure did not produce readily observable microstructural degradation or chemical modifications. Consequently, any hydrogen-induced changes are likely to have occurred at a sub-microscopic scale below the resolution of the employed characterisation techniques.

While such defects may have a negligible influence on monotonic tensile behaviour, where failure is governed by the ability of the composite to withstand a single increasing load, they can become significantly more detrimental under cyclic loading conditions. Fatigue loading repeatedly activates local stress concentrations, facilitating the initiation and progressive growth of matrix cracks, interfacial damage, and delaminations. Consequently, even subtle changes in the defect population or in the integrity of the fibre–matrix interface may lead to a measurable reduction in fatigue life without producing a corresponding decrease in static strength.

This interpretation is also consistent with the well-established observation that the fatigue performance of composite materials is generally more sensitive to defects and microstructural heterogeneities than their monotonic tensile strength [31, 32]. Therefore, it is plausible that hydrogen exposure introduced or enhanced damage features that remained undetectable through the analyses conducted in this work, yet were sufficient to accelerate fatigue damage accumulation. From this perspective, the present observations suggest that

the primary effect of hydrogen exposure is not a direct reduction in the static load-carrying capability of the material, but rather a modification of the mechanisms governing damage initiation and propagation during cyclic loading. Since it is possible that subtle or sub-microscopic effects were not captured by the analyses discussed above, further microscale investigations are required to elucidate the mechanisms responsible for the observed reduction in fatigue endurance.

The above interpretations are consistent with the observed mechanical behaviour, the microstructural evidence gathered in the present study, and the current understanding of hydrogen effects in CFRP systems. Nevertheless, further investigations employing dedicated microscale characterisation techniques would be valuable to establish the precise mechanisms by which hydrogen influences matrix and fibre–matrix interface damage evolution.

6. Implications of Hydrogen Exposure for Fatigue Design

By combining the static and fatigue results, the influence of hydrogen on the T700/VTC401 $[0]_{2s}$ laminate can be summarised as follows. Under static loading, hydrogen soaking does not significantly modify the tensile response at the coupon scale. Within experimental scatter, the elastic modulus and ultimate tensile strength of hydrogen-soaked specimens are comparable to those of the unsoaked material, indicating no systematic degradation of static tensile properties. Because the monotonic tensile strength and modulus (i.e., fibre-dominated properties) remained unchanged following hydrogen exposure, the present results provide no evidence of hydrogen-induced degradation of the carbon fibres. This interpretation is further supported by the absence of distinctive fibre-related features in the microscopic examinations and by previous studies reporting the limited sensitivity of carbon fibres to hydrogen exposure [17]. Accordingly, the observed fatigue degradation is more likely to be associated with subtle changes occurring within the polymer matrix and/or at the fibre–matrix interface rather than with damage to the fibres themselves. In contrast, under cyclic loading at $R = 0.1$, hydrogen exposure has a clear detrimental effect on fatigue performance. The endurance limit decreases in absolute terms, and the S–N curve becomes flatter, indicating that the adverse effect of hydrogen becomes increasingly pronounced as operating conditions shift from the high-cycle towards the medium-cycle fatigue regime. The increase in the inverse slope parameter from 45.0 for the unsoaked condition to 59.6 following hydrogen exposure suggests that the detrimental effect of hydrogen becomes increasingly pronounced as the applied stress amplitude increases. A possible explanation is that hydrogen promotes the formation or exacerbation of localised defects within the polymer matrix and at the fibre–matrix interface. Although such defects may remain undetectable through the characterisation techniques employed in the present study, they can act as local stress concentrators and preferential sites for damage initiation. As the magnitude of the applied cyclic stress increases, the corresponding local stresses and strains in the vicinity of these defects also increase, accelerating matrix cracking, fibre–matrix debonding, and the subsequent development of delaminations. Consequently, hydrogen-induced defects may have a disproportionately greater influence on fatigue life in the medium-cycle fatigue regime than at lower stress amplitudes, resulting in a steeper reduction in life with increasing stress and, therefore, a larger value of the inverse slope parameter. While this interpretation remains a hypothesis, it is consistent with both the observed fatigue behaviour and the absence of measurable changes in the static tensile properties.

From a design perspective, reliance on static tensile properties alone is therefore insufficient for components operating in gaseous hydrogen. Although the hydrogen-soaked laminate retains static properties broadly similar to the unsoaked material, the usable fatigue strength

at a given probability of survival is significantly reduced, and a lower allowable stress amplitude of the order of 10–15% at $N_A = 2 \times 10^6$ cycles is required in hydrogen to achieve comparable endurance. The absence of a marked increase in the scatter ratio T_σ is nevertheless encouraging, as it suggests that hydrogen primarily shifts the mean S–N curve to a more critical position without introducing substantial additional variability in fatigue life. Overall, these findings confirm that hydrogen degradation in this laminate is fundamentally a fatigue-driven, matrix/interface-controlled process, with clear implications for structural integrity assessment and for the derivation of hydrogen-specific S–N design curves and safety factors for long-term gaseous hydrogen service.
These trends are specific to the T700/VTC401 $[0]_{2s}$ laminate tested at room temperature, low hydrogen pressure and $R = 0.1$; extension to other lay-ups, loading ratios and environmental conditions will require further work.

7. Conclusions

An experimental investigation was conducted to assess the effect of long-term gaseous hydrogen exposure on the static and fatigue behaviour of T700/VTC401 $[0]_2$s CFRP laminates. Specimens were soaked in 6 bar hydrogen at room temperature for 10 months and compared with unsoaked reference coupons. Based on the results obtained, the following conclusions can be drawn:

1. Long-term hydrogen exposure did not produce any measurable degradation in the fibre-direction tensile properties of the investigated laminate. The elastic modulus and ultimate tensile strength of the hydrogen-soaked material remained comparable to those of the unsoaked condition.
2. Hydrogen exposure resulted in a clear reduction in fatigue performance under tension–tension loading (R = 0.1). In particular, the endurance limit at 2×10⁶ cycles decreased by approximately 10%, demonstrating that hydrogen can adversely affect the fatigue resistance of CFRP laminates even when their static tensile properties remain unchanged.
3. The hydrogen-soaked material exhibited a flatter S–N response than the unsoaked condition, indicating an increased sensitivity of fatigue life to stress amplitude in the medium- and high-cycle fatigue regimes.
4. Optical microscopy, Raman spectroscopy, and secondary electron microscopy did not reveal any distinctive hydrogen-related changes in surface morphology, fracture features, or material structure. The observed fatigue degradation therefore appears to be associated with subtle hydrogen-induced modifications occurring at scales below the resolution of the characterisation techniques employed.
5. The results highlight the importance of assessing fatigue performance when qualifying CFRP materials for hydrogen-service applications. Static tensile properties alone may not provide a sufficient basis for evaluating the structural integrity of hydrogen-exposed composite components.

Further microscale investigations are required to clarify the mechanisms responsible for the observed reduction in fatigue endurance.

Acknowledgments

The contribution from Jonathan Duff for conducting the exposure in hydrogen environments is acknowledged. This work was also supported by the Henry Royce Institute for Advanced Materials, funded through EPSRC grants EP/R00661X/1 and EP/P025021/1.

References

[1] Bhuiyan MMH, Subedi N, Siddique Z. Material compatibility in hydrogen infrastructure: Challenges, advances, and future prospects. Int J Hydrogen Energy 2025;190. https://doi.org/10.1016/j.ijhydene.2025.152138.

[2] Zhang M, Lv H, Kang H, Zhou W, Zhang C. A literature review of failure prediction and analysis methods for composite high-pressure hydrogen storage tanks. Int J Hydrogen Energy 2019;44:25777–99. https://doi.org/10.1016/j.ijhydene.2019.08.001.

[3] Li M, Bai Y, Zhang C, Song Y, Jiang S, Grouset D, et al. Review on the research of hydrogen storage system fast refueling in fuel cell vehicle. Int J Hydrogen Energy 2019;44:10677–93. https://doi.org/10.1016/j.ijhydene.2019.02.208.

[4] Zhou W, Wang J, Pan Z bo, Liu J, Ma L hua, Zhou J yi, et al. Review on optimization design, failure analysis and non-destructive testing of composite hydrogen storage vessel. Int J Hydrogen Energy 2022;47:38862–83. https://doi.org/10.1016/j.ijhydene.2022.09.028.

[6] Sun WX, Li YT, Huang WJ, Zhang YM, Fan M, Xiao ZM, et al. Advances in failure assessment of Type IV hydrogen storage vessels: A critical review. Renewable and Sustainable Energy Reviews 2026;226. https://doi.org/10.1016/j.rser.2025.116353.

[7] Wang L, Wang B, Wei S, Hong Y, Zheng C. Prediction of long-term fatigue life of CFRP composite hydrogen storage vessel based on micromechanics of failure. Compos B Eng 2016;97:274–81. https://doi.org/10.1016/j.compositesb.2016.05.012.

[8] Wu E, Zhao Y, Zhao B, Xu W. Fatigue life prediction and verification of high-pressure hydrogen storage vessel. Int J Hydrogen Energy 2021;46:30412–22. https://doi.org/10.1016/j.ijhydene.2021.06.177.

[9] Feki I, Shirinbayan M, Nouira S, Bi RT, Maeso JB, Thomas C, et al. Multi-scale fatigue damage analysis in filament-wound carbon fiber reinforced epoxy composites for hydrogen storage tanks. Composites Part C: Open Access 2024;15. https://doi.org/10.1016/j.jcomc.2024.100537.

[10] Ma L, Liu C, Han J, Wen A, Liu B, Zheng J. Delamination defects in composite hydrogen storage cylinders: CT scanning and shearography measurement. Int J Hydrogen Energy 2025;97:140–9. https://doi.org/10.1016/j.ijhydene.2024.11.447.

[11] Oz FE, Wagih A, Joarder B, Datta SJ, Eddaoudi M, Lubineau, G. Microstructure-driven hydrogen permeability in thin-ply thermoplastic composites: Insights for Type V storage tanks. Compos Part A Appl Sci Manuf 2026;200:109316 - https://doi.org/10.1016/j.compositesa.2025.109316

[12] Wagih A, Oz FE, Melentiev R, Mahmoud HA, Maimí P, Abdelaziz M, Lubineau G. Advancing safety of hydrogen polymeric tanks: A review of permeation mitigation, leak detection, and smart monitoring. Int J Hydrog Energy 2025;176:151334 - https://doi.org/10.1016/j.ijhydene.2025.151334

[13] Okumuş M, Janssen F, Figiel Ł. Modelling and experimental study of hydrogen permeation in polymer composites: Effects of fibre agglomeration and orientation. Compos Part A Appl Sci Manuf 2025;199. https://doi.org/10.1016/j.compositesa.2025.109213.

[14] Gao Y, Peng C, Chen W, Liu Z, Liu S. Advances and prospects of failure modes in key hydrogen-related components within the hydrogen energy supply chain. Int J Hydrog Energy 2025;130:503-519 - https://doi.org/10.1016/j.ijhydene.2025.04.333

[15] Bodaghi, M. et al. A review of technical challenges and research gaps to address permeability controls in cryogenic composite hydrogen tanks. Composites Part B: Engineering 2026;315:113427 - https://doi.org/10.1016/j.compositesb.2026.113427

[16] Katsivalis I, Signorini V, Ohlsson F, Langhammer C, Minelli M, Asp LE. Hydrogen permeability of thin-ply composites after mechanical loading. Compos Part A Appl Sci Manuf 2024;176. https://doi.org/10.1016/j.compositesa.2023.107867.

[17] Jeon SK, Kwon OH, Jang HS, Ryu KS, Nahm SH. Effect of high pressure hydrogen on the mechanical characteristics of single carbon fiber. Applied Surface Science 2018;432(B):176-182. https://doi.org/10.1016/j.apsusc.2017.07.005
[18] Li S, Qiu K, Wang Z, Zhao S, Wan Z. Static and fatigue behaviors of epoxy-based sealing layers for underground hydrogen energy storage. Int J Hydrogen Energy 2024;60:66–81. https://doi.org/10.1016/j.ijhydene.2024.02.059.
[19] Kumar, M. Investigation of Hydrogen Transport Properties through the Liner Material of 70 MPa Type IV Composite Overwrapped Pressure Vessels. International Journal of Pressure Vessels and Piping 2024;208:105150 - https://doi.org/10.1016/j.ijpvp.2024.105150
[20] ASTM D3039/D3039M-17. Standard Test Method for Tensile Properties of Polymer Matrix Composite Materials. ASTM International, West Conshohocken, PA; 2017. https://doi.org/10.1520/D3039_D3039M-17R25.
[21] ASTM D3479/D3479M-19. Standard Test Method for Tension–Tension Fatigue of Polymer Matrix Composite Materials. ASTM International, West Conshohocken, PA; 2023. https://doi.org/10.1520/D3479_D3479M-19R23.
[22] Broughton WR, Lodeiro MJ. Fatigue testing of composite laminates. NPL Report CMMT(A)252. Teddington (UK): National Physical Laboratory; 2000.
[23] ASTM E739. Standard Practice for Statistical Analysis of Linear or Linearized Stress-Life (S-N) and Strain-Life (ε-N) Fatigue Data. ASTM International, West Conshohocken, PA; 2023. https://doi.org/10.1520/E0739-23.
[24] Kufoin E, Susmel L. Quantitative review of probabilistic approaches to fatigue design in the medium cycle fatigue regime. Probabilistic Engineering Mechanics 2024;75. https://doi.org/10.1016/j.probengmech.2024.103589.
[25] Kufoin E, Susmel L. On the parametric assessment of fatigue disparities. Probabilistic Engineering Mechanics 2024;77. https://doi.org/10.1016/j.probengmech.2024.103651.
[26] King JE. Failure in composite materials[J]. Metals and materials, 1989, 5(12): 720-726.
[27] Smoleń J, Olesik P, Jała J, Adamcio A, Kurtyka K, Godzierz M, et al. The Use of Carbon Fibers Recovered by Pyrolysis from End-of-Life Wind Turbine Blades in Epoxy-Based Composite Panels. Polymers (Basel) 2022;14. https://doi.org/10.3390/polym14142925.
[28] Vašková H, Křesálek V. Raman spectroscopy of epoxy resin crosslinking. In: ACMOS'11: Proceedings of the 13th WSEAS international conference on Automatic control, modelling & simulation. V. Vasek, Y. Shmaliy, D. Trcek, N. P. Kobayashi, R. S. Choras, Eds. Canary Islands, Spain, May 27 - 29, 2011, pp. 357-361. ISBN: 978-1-61804-004-6.
[29] Barth, R. R. et al. Polymers for hydrogen infrastructure and vehicle fuel systems. Technical Report, Sandia National Laboratories (SNL-CA), Livermore, CA, US, 2013. https://doi.org/10.2172/1104755
[30] Ding, G. et al. Molecular study of high-pressure hydrogen decompression in amorphous polyethylene. Int J Hydrog Energy 2025;114:267-278 - https://doi.org/10.1016/j.ijhydene.2025.03.056
[31] Sisodia S, Gamstedt EK, Edgren F, Varna J. Effects of voids on quasi-static and tension fatigue behaviour of carbon-fibre composite laminates. J Compos Mater 2015;49(17):2137-2148. https://doi.org/10.1177/0021998314541993
[32] Maragoni L, Carraro PA, Quaresimin M. Prediction of fatigue life to crack initiation in unidirectional plies containing voids. Compos - A: Appl Sci Manuf 2019;127:105638. https://doi.org/10.1016/j.compositesa.2019.105638.

List of Captions

Figure 1. Images from the panel manufacturing process. A: prepreg layup, B application of the release film, C: vacuum bagging, D: autoclave cure.

Figure 2. Diagram of the laminate with end-tab strips positioned and overlay of waterjet cuts.

Figure 3. Hydrogen pressure tube system.

Figure 4. Representative stress–strain curves for (a) an unsoaked laminate specimen (Test No. 1) and (b) a hydrogen-soaked laminate specimen (Test No. 4).

Figure 5. S-N curves for unsoaked and H_2-soaked T700/VTC401 $[0]_{2s}$ specimens.

Figure 6. Tool-face surface of unsoaked and H_2-soaked T700/VTC401 $[0]_{2s}$ laminate specimen.

Figure 7. Bag-face surface of unsoaked and H_2-soaked T700/VTC401 $[0]_{2s}$ laminate specimen.

Figure 8. Fracture surface of unsoaked and H_2-soaked T700/VTC401 $[0]_{2s}$ laminate specimen tested under fatigue loading.

Figure 9. Optical images of the Raman-mapped regions for the (a) unsoaked (VTC-11-1750) and (b) soaked composites (VTCH3-1500).

Figure 10. Individual Raman spectra collected along the line map for the (a) unsoaked (VTC-11-1750) and (b) hydrogen-soaked composites (VTCH3-1500) post fatigue test.

Figure 11. Mean Raman spectra for the unsoaked (VTH-11-1750) and the soaked (VTCH3-1500) fatigue composites (in red and blue, respectively), averaged over the mapped regions.

Figure 12. SEM micrographs showing fracture surfaces of unsoaked and H_2-soaked T700/VTC401 $[0]_{2s}$ laminate specimens under static (a) and fatigue (b) loading.

Table 1 Mechanical properties of hydrogen-soaked and unsoaked T700/VTC401 $[0]_{2s}$ specimens.

Figures

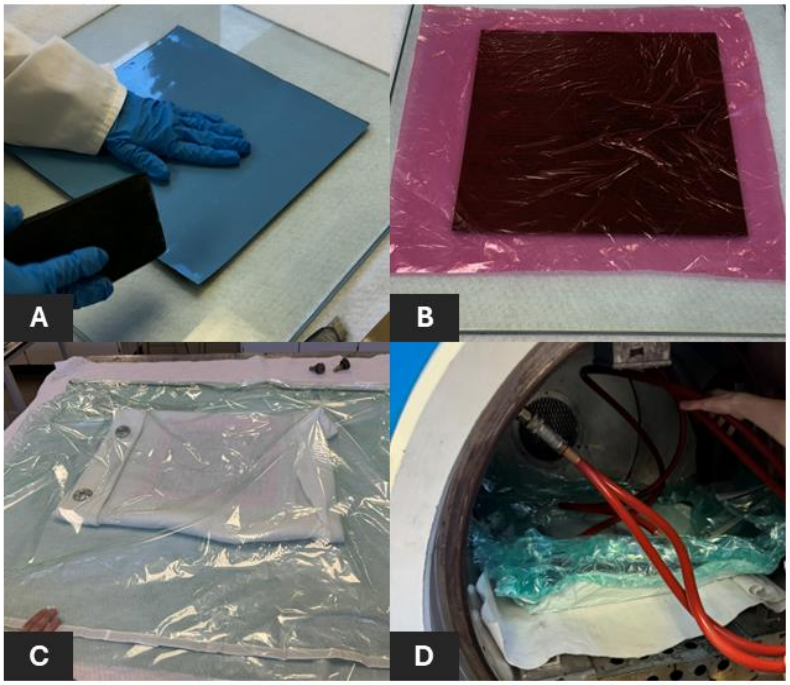

Figure 1. Images from the panel manufacturing process. A: prepreg layup, B application of the release film, C: vacuum bagging, D: autoclave cure.

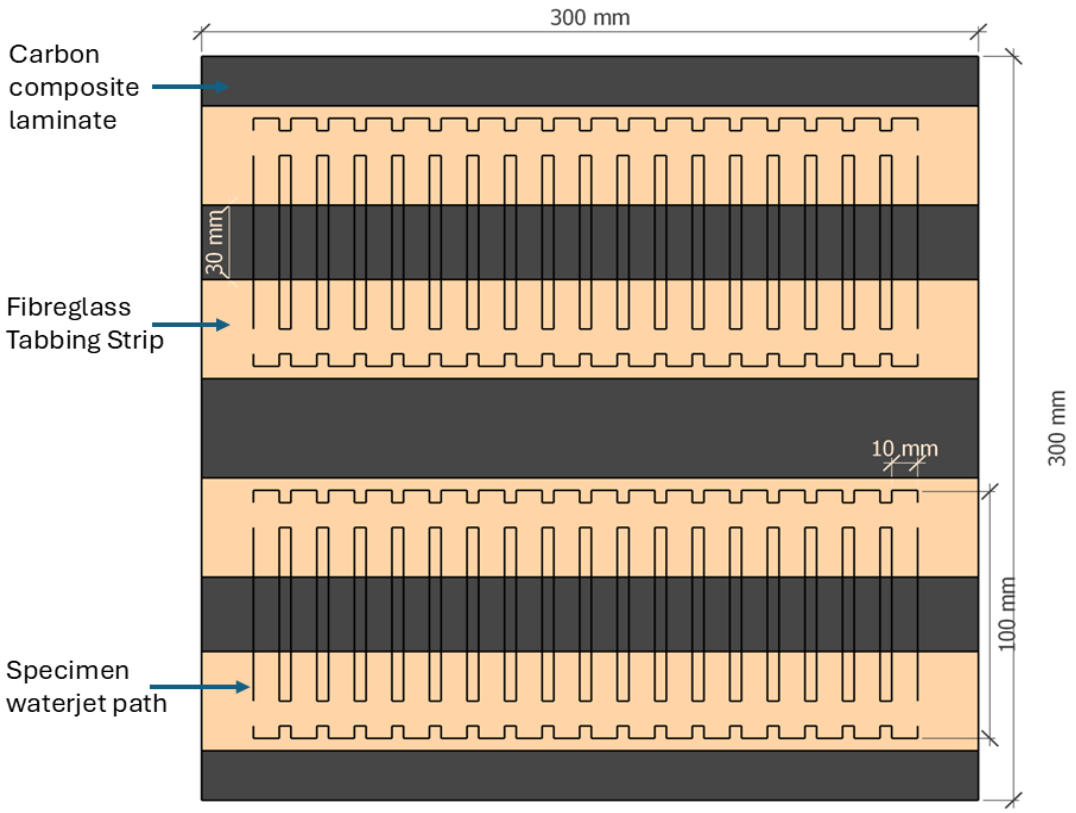

Figure 2. Diagram of the laminate with end-tab strips positioned and overlay of waterjet cuts.

Figure 3. Hydrogen pressure tube system.

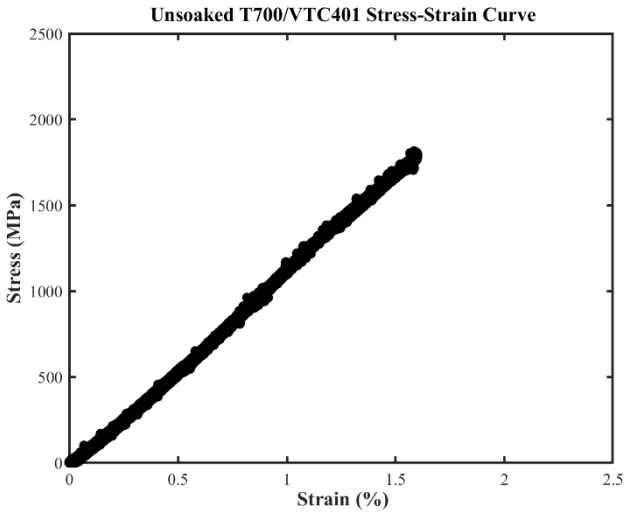

(a)

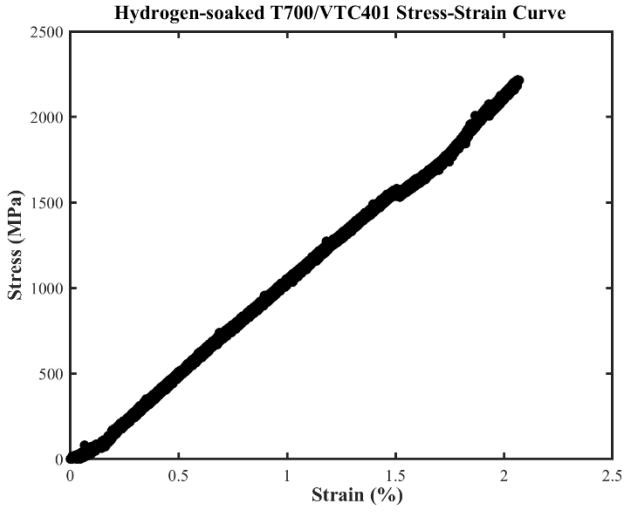

(b)

Figure 4. Representative stress–strain curves for (a) an unsoaked laminate specimen (Test No. 1) and (b) a hydrogen-soaked laminate specimen (Test No. 4).

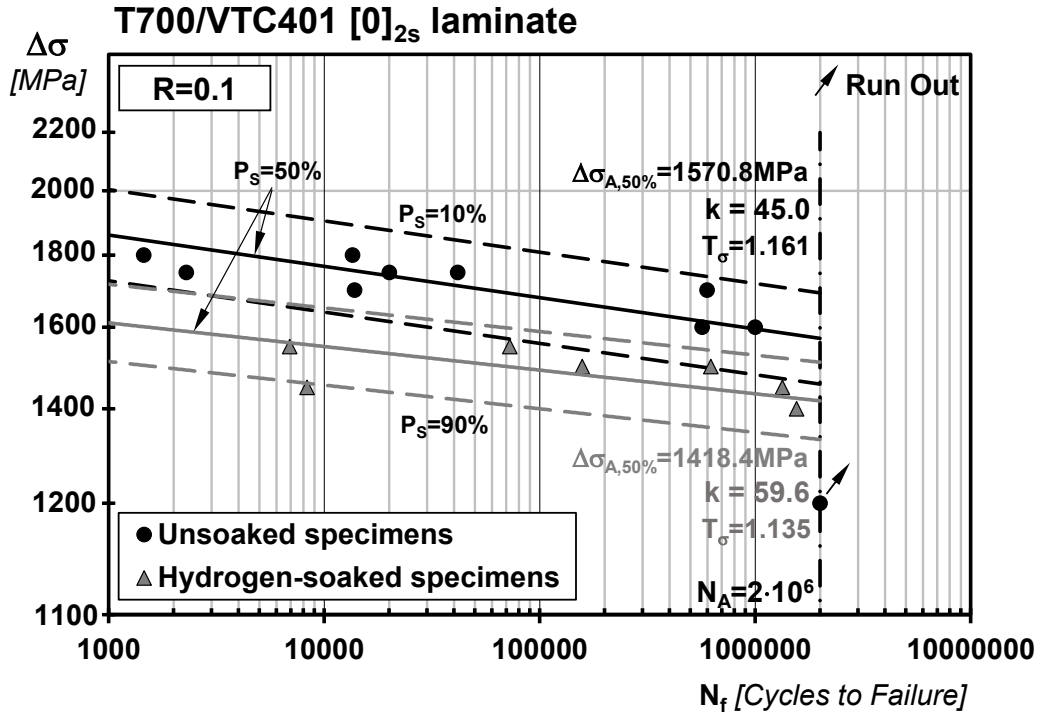

Figure 5. S-N curves for unsoaked and H_2-soaked T700/VTC401 $[0]_{2s}$ specimens.

Unsoaked	Hydrogen soaked
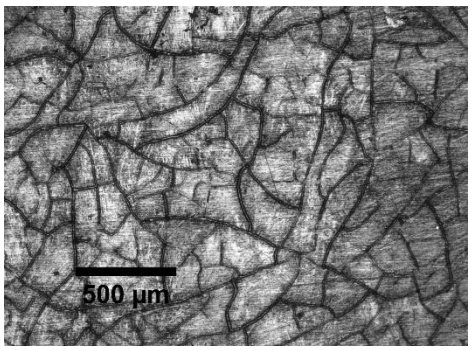	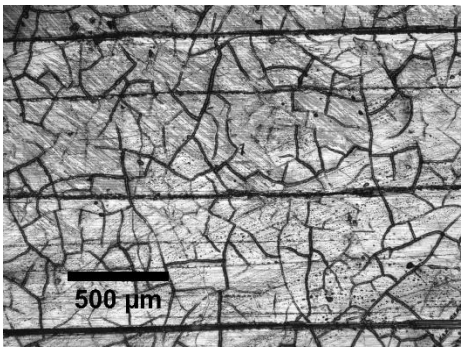
T700VTC_1 – Magnification: **5x**	T700VTCH_2– Magnification: **5x**
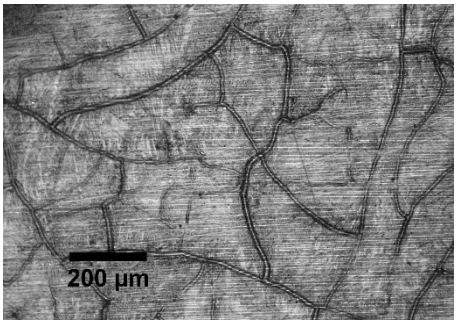	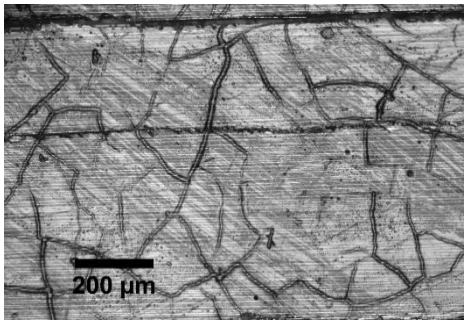
T700VTC_1 – Magnification: **10x**	T700VTCH_2 – Magnification: **10x**
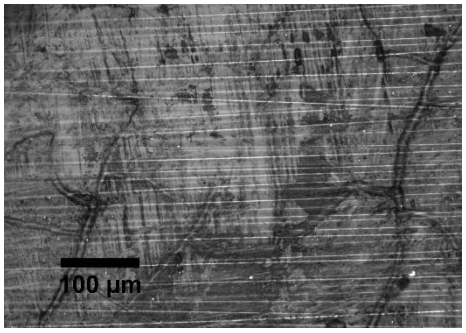	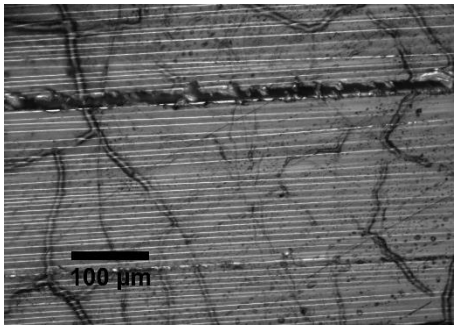
T700VTC_1 – Magnification: **20x**	T700VTCH_2 – Magnification: **20x**

Figure 6. Tool-face surface of unsoaked and H_2-soaked T700/VTC401 $[0]_{2s}$ laminate specimen.

Unsoaked	Hydrogen soaked
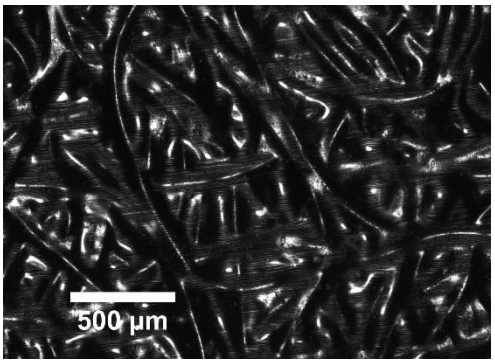	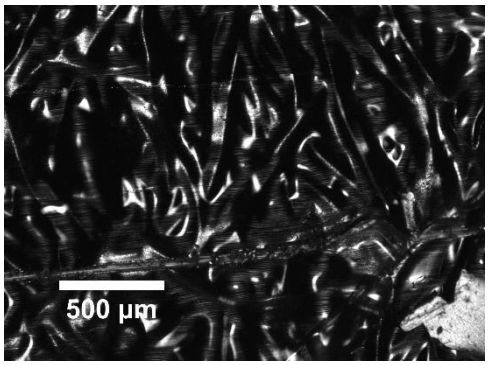
T700VTC_1 – Magnification: **5x**	T700VTCH_2 – Magnification: **5x**
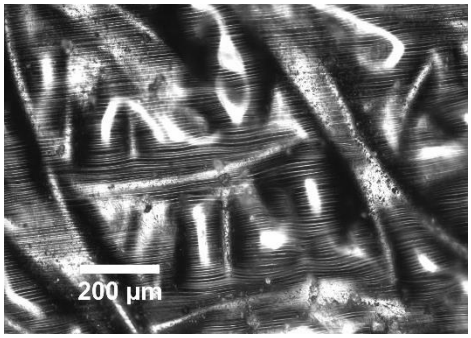	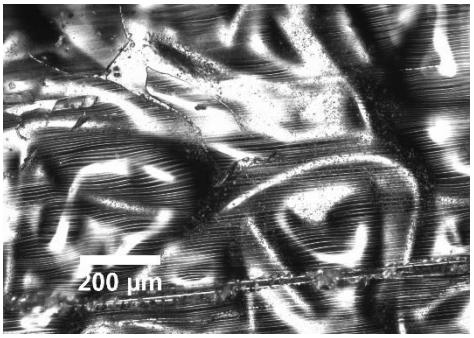
T700VTC_1 – Magnification: **10x**	T700VTCH_2 – Magnification: **10x**
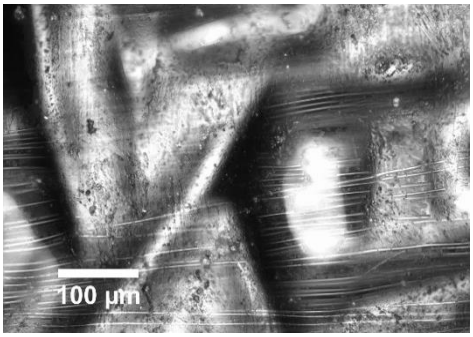	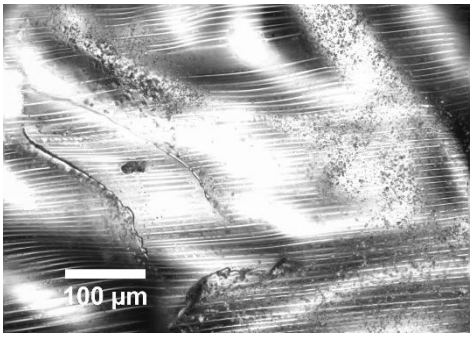
T700VTC_1 – Magnification: **20x**	T700VTCH_2 – Magnification: **20x**

Figure 7. Bag-face surface of unsoaked and H_2-soaked T700/VTC401 $[0]_{2s}$ laminate specimen.

Unsoaked	Hydrogen soaked
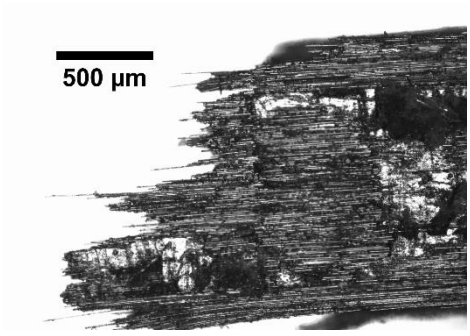	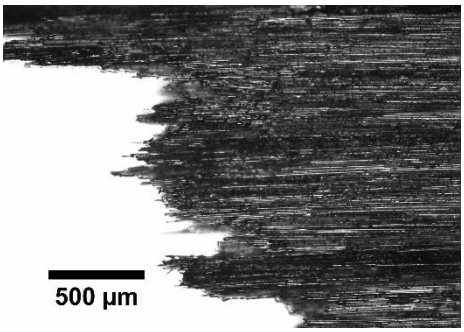
T700VTC_11 - Magnification: **5x**	T700VTCH_3- Magnification: **5x**
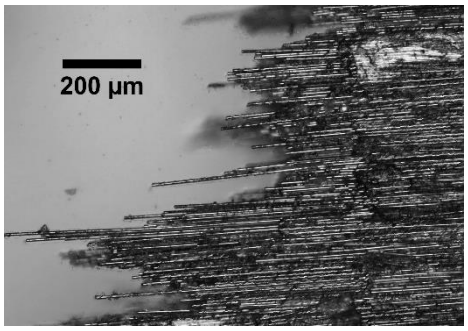	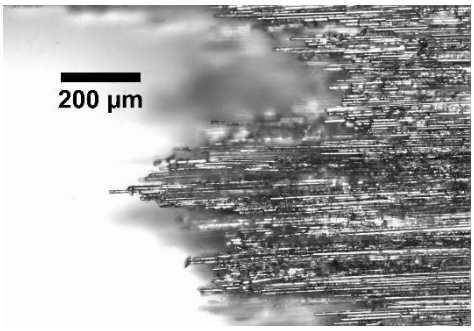
T700VTC_11 - Magnification:**10x**	T700VTCH_3 - Magnification: **10x**

Figure 8. Fracture surface of unsoaked and H_2-soaked T700/VTC401 $[0]_{2s}$ laminate specimen tested under fatigue loading.

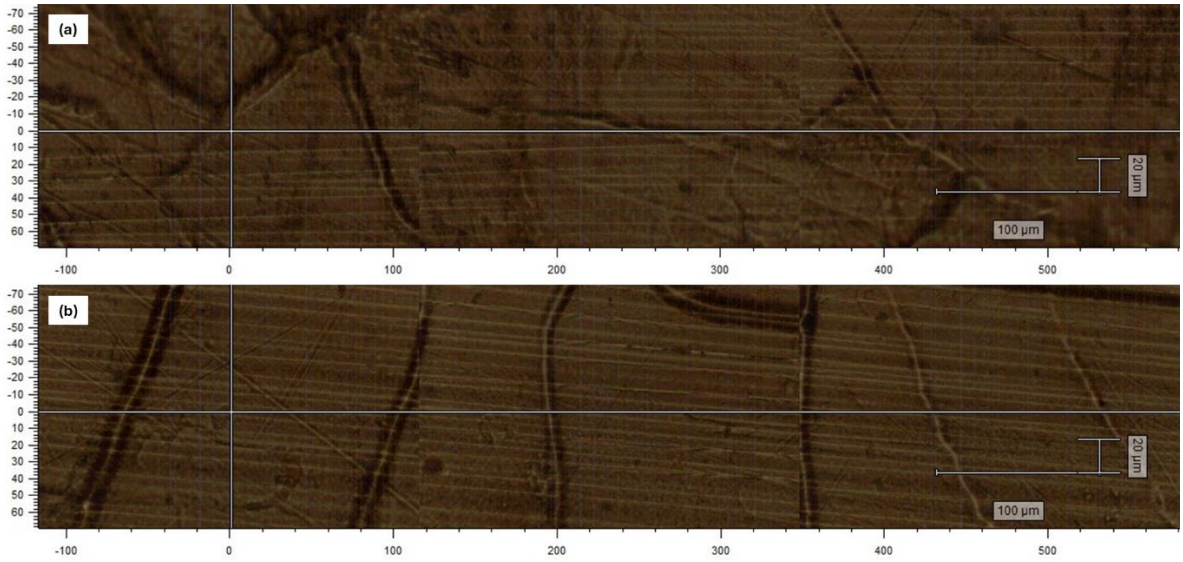

Figure 9. Optical images of the Raman-mapped regions for the (a) unsoaked (VTC-11-1750) and (b) soaked composites (VTCH3-1500).

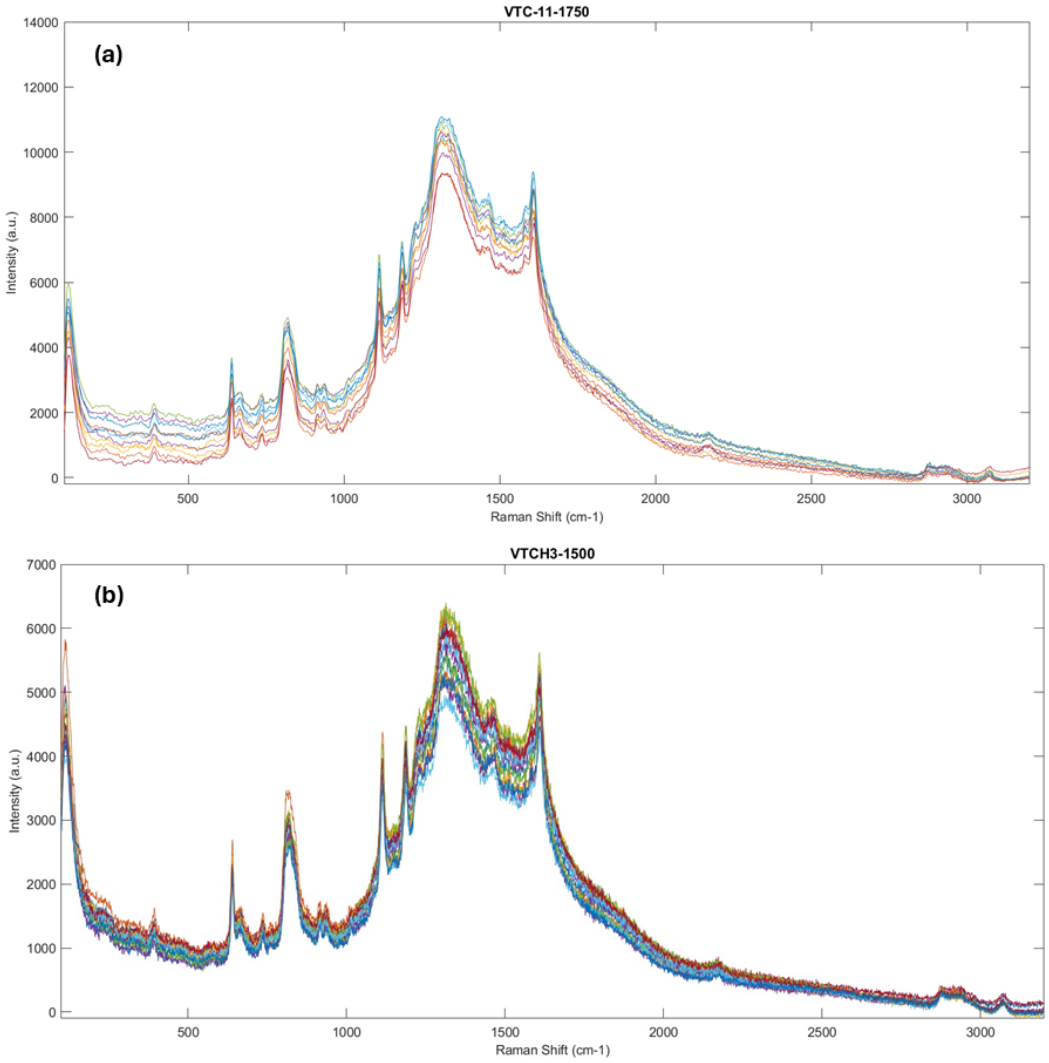

Figure 10. Individual Raman spectra collected along the line map for the (a) unsoaked (VTC-11-1750) and (b) hydrogen-soaked composites (VTCH3-1500) post fatigue test.

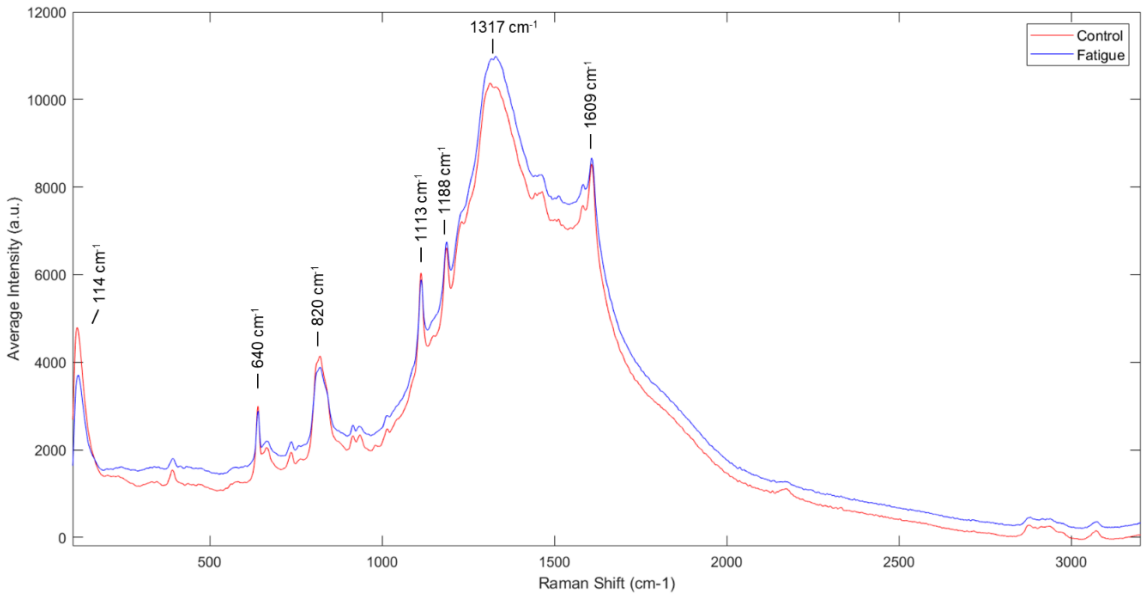

Figure 11. Mean Raman spectra for the unsoaked (VTH-11-1750) and the soaked (VTCH3-1500) fatigue composites (in red and blue, respectively), averaged over the mapped regions.

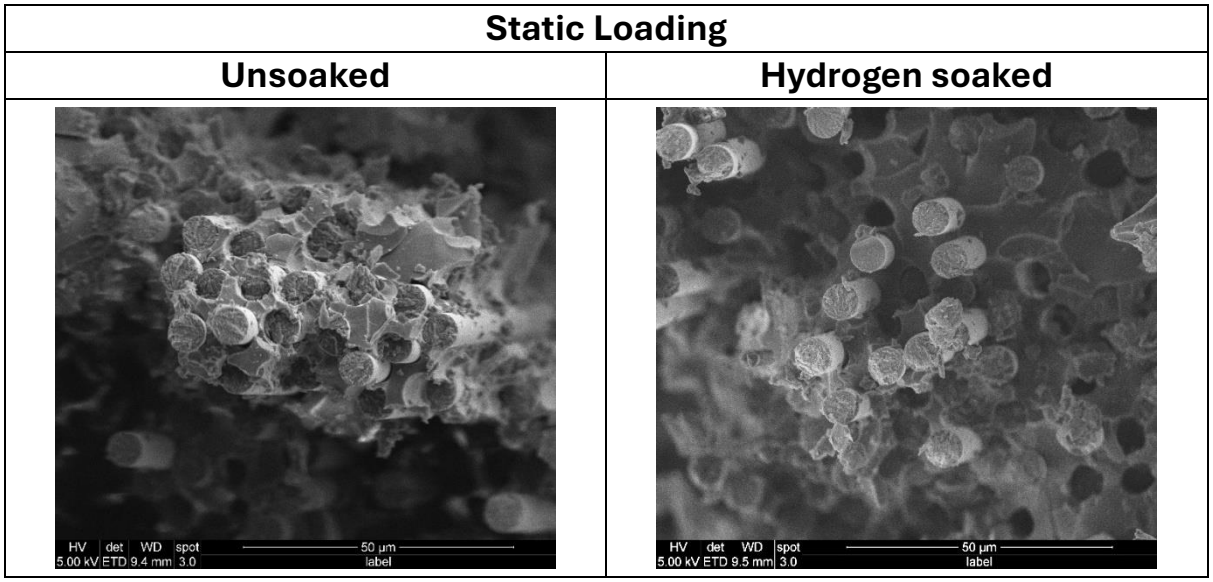

(a)

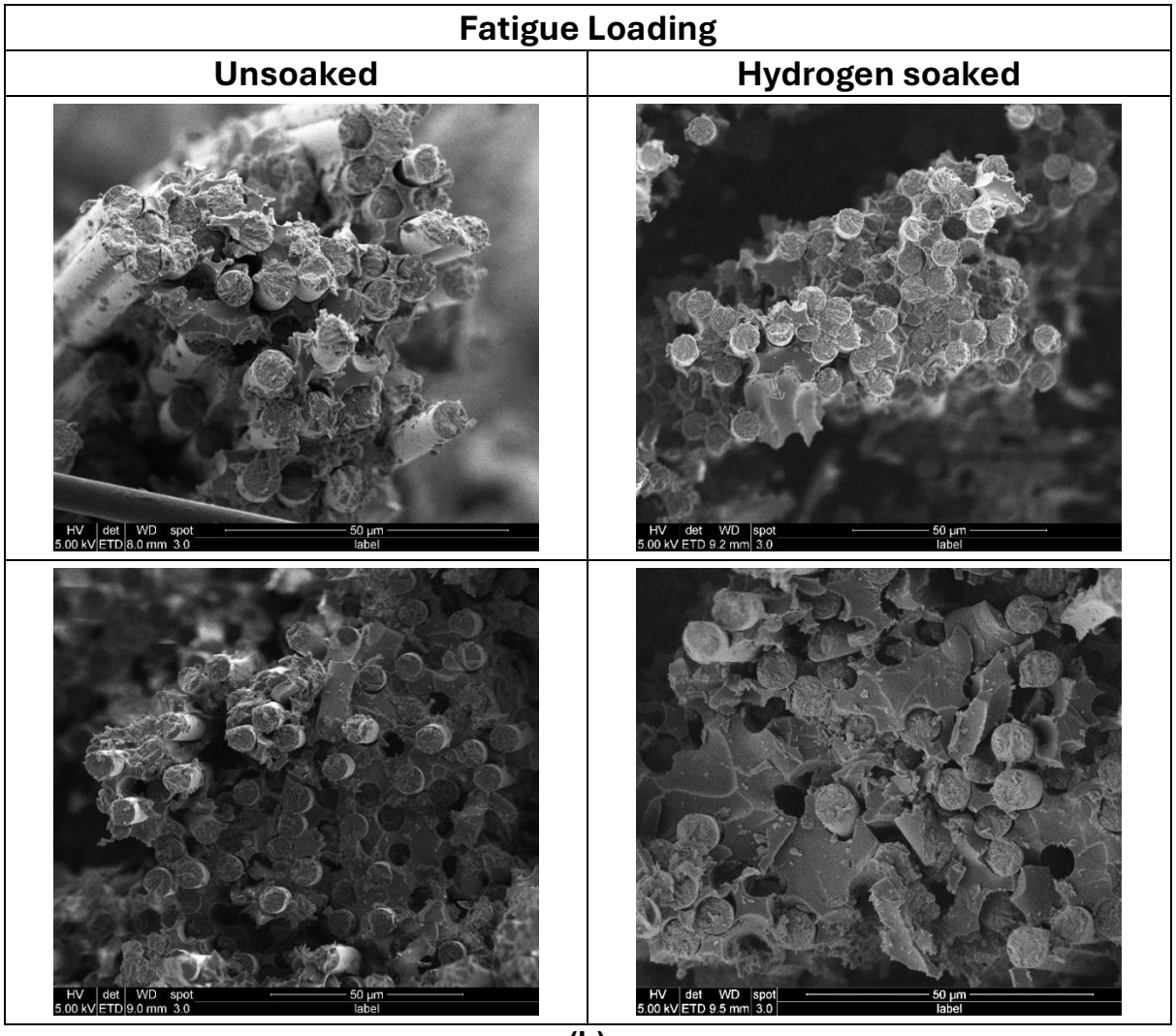

(b)

Figure 12. SEM micrographs showing fracture surfaces of unsoaked and H_2-soaked T700/VTC401 $[0]_{2s}$ laminate specimens under static (a) and fatigue (b) loading.

Tables

Table 1 Mechanical properties of hydrogen-soaked and unsoaked T700/VTC401 $[0]_{2s}$ specimens.

No. of tests	Soaking condition	E [GPa]	σ_{UTS}[MPa]
1	Un-soaked	107.8	1818.7
2		120.8	2193.6
3		105.2	2132.1
4	H_2-soaked	115.4	2222.8
5		106.0	2187.6